International Journal of ChemTech Research
CODEN (USA): IJCRGG, ISSN: 0974-4290, ISSN(Online):2455-9555
Vol.11 No.10, pp 33-40, 2018

Activated carbon-doped with iron oxide nanoparticles (α-Fe_2O_3 NPs) preparation: particle size, shape, and impurity

Settakorn Upasen

Department of Chemical Engineering, Faculty of Engineering, Burapha University, 169 Long-Hard Bangsaen Road, Saensook District, Muang, Chonburi, 20131 Thailand

Abstract : Inspired by the development of an adsorbent material with a high capacity for chlorinated gas treatment, an α-Fe_2O_3 nanoparticle deposited activated carbon adsorbent was successfully synthesized. The α-Fe_2O_3 NPs synthesis was done by a facile chemical precipitation method using sodium hydroxide (NaOH) as a precipitant agent. The variation of the molar ratio of the reactant and precipitant (i.e. 1:1, 1:1.5, 1:2 by mole) and of the precipitating temperature (i.e. 50, 70, 90°C) were explored. The physical and chemical characteristics of the synthesized samples were examined using various techniques; Transmission Electron Microscope (TEM), Brunauer-Emmett-Teller analysis (BET), Thermogravimetry analysis (TGA), Fourier Transform Infra-Red (FT-IR) and Ultraviolet-Visible spectrophotometer. The result shows that two synthesized conditions - 1:1 by mole ($FeCl_3$:NaOH) at 70°C and 1:1.5 by mole ($FeCl_3$:NaOH) at 90°C -were allowed to produce the smallest size of α-Fe_2O_3 NPs approximately 10 nm. Consequently, it gave the highest specific surface area of ~110 m^2/g. With a higher $FeCl_3$: NaOH molar ratio and a higher precipitating temperature, the synthesized Fe_2O_3 NPs formed a more oval shape with a finer surface. Due to the insufficient purification, unfortunately, an impurity caused by sodium salt was detected in the amount of 5-10 wt.%. The minimum amount of 75 wt.% α-Fe_2O_3 NPs coated on the activated carbon was observed. The production yield of the synthesized α-Fe_2O_3 and α-Fe_2O_3/GAC samples was also reported.

Keywords : Iron oxide (α-Fe_2O_3), nanoparticle, activated carbon, synthesis, characterization.

Introduction

Activated carbon - a material having an abundant porous structure and strong adsorption capacity - produced from various sources such as sugarcane bagasse, coconut shell, longan seed, apricot kernel, bamboo. The activated carbon can be used in many different applications including; separation, removal of dyes and pollutants from gas/wastewater, and as a catalyst support. Although the activated carbon is capable of adsorbing many kinds of pollutants i.e. chromium (V)[1-3], chlorinated gas [4, 5], dyes [6], its adsorption efficiency and adsorption capacity are limited. These disadvantages restrict its extensive application. Several studies have

DOI= http://dx.doi.org/10.20902/IJCTR.2018.111006

modified the activated carbon by depositing metals and/or metal oxide i.e. nano-zerovalent iron [3], iron oxide [7, 8], cerium [6]. In this paper, we are interested in preparing ferric oxide (Fe_2O_3) coated on the surface/porous of the activated carbon adsorbent.

Ferric (III) oxide (Fe_2O_3) is a low cost, stable and environmentally-friendly compound. It can exist in the γ phase (maghemite) or α phase (hematite). The hematite is widely used for catalysts [9, 10], inorganic pigments [11-14], water treatments[15-17] and, lithium-ion batteries [18-20]. In order to prepare the hematite nanoparticle, several synthesis methods were studied i.e. sol-gel method[21, 22], hydrothermal [23, 24], precipitation [25-28], non-thermal/thermal plasma [29, 30], etc. The selection of such different methods was dependent upon their applications. Consequently, size, shape, and purity of the hematite compound varies depending on the synthesis parameters such as; reactant concentration [25], pH solution [27], reaction time and temperature, and the nature of the iron salts [28]. The hematite is commonly found in a rhombohedral (hexagonal) structure [25]. A number of morphology characteristics have been reported i.e. sphere [25, 26, 28], snowflake-like [29], or rods [31] with a particle size of a few to several hundred nanometers.

In the present study, we prepared and characterized hematite nanoparticles. Activated carbon was doped with hematite nanoparticles via a facile chemical precipitation method. We have also attempted to explore the effect of the precipitant amount and the precipitating temperature on hematite nanoparticles' size and shape.

Sample and Methods

Synthesis

Hematite nanoparticles (α-Fe_2O_3 NPs) were synthesized by a chemical precipitation method. A 2 M ferric chloride ($FeCl_3$) aqueous solution was prepared by dissolving it in 100 mL of deionized distilled water. An amount of 25 mL of the $FeCl_3$ aqueous solution was contained in a 2-necks round and flat-bottom vessel and stirred at 300 rpm under a 50°C precipitating temperature for 30 minutes. Then, an amount of 9.3 mL of 5.4 M NaOH precipitation agent was slowly added. The mixture remained stirring for 5 minutes. To proceed the sedimentation process, we installed a facile reflux condenser into the reactor vessel, the temperature was heated up to 90°C, and stirred for 3 hours. The brown precipitation was received. Then it was centrifuged and washed with distilled water several times. The collected precipitates were dried in air at 105°C for 12 hours. Note that the collected precipitates were named as a pre-calcined sample. Finally, the pre-calcined samples were calcined at 350°C for 4 hours. To explore the impact of the added NaOH amount and the precipitating temperature, Table 1 illustrates the synthesized parameters for Fe_2O_3 NPs and GAC/Fe_2O_3.

Activated carbon used in this study was in a granular form, GAC, supported by the Carbokarn Co., Ltd., Thailand. The source of GAC was from a coconut shell. The particle size of the as-received GAC was 4.75 – 2.36 mm in diameter. With the test of BET-surface area using Quantachrome NOVA 1200, the as-received GAC shows 93.7 m^2/g.

Table 1. The synthesized parameters of Fe_2O_3 NPs and GAC/Fe_2O_3 NPs preparation

Sample	Activated carbon(g)	Molar Ratio ($FeCl_3$:NaOH)	Amount of NaOH (mL)	Precipitating Temp. (°C)
S1	-	1.0 : 1.0	9.3	50
S2	-	1.0 : 1.0	9.3	70
S3	-	1.0 : 1.0	9.3	90
S4	-	1.0 : 1.5	13.9	90
S5	-	1.0 : 2.0	18.6	90
GAC/Fe1	1	1.0 : 1.5	13.6	70
GAC/Fe2	2	1.0 : 1.5	13.6	70
GAC/Fe3	3	1.0 : 1.5	13.6	70

Characterization

TEM and SEM measurements

Morphology characteristics of the synthesized samples were analyzed by the scanning electron microscopy (SEM) LEO1450VP, the 15kV type with resolution 71,000x-13,000x. In addition, the transmission electron micrographs of the synthesized Fe_2O_3 NPs were obtained using the transmission electron microscope (TEM), Phillip-Tecnai20, at 100 kV with a resolution of 13,5000x – 13,000x. In order to prepare the analyzed sample with well-dispersed particles, the hematite powders were dissolved in ethanol solution and sonicated for several minutes.

BET analysis

In order to analyze the specific surface area of the synthesized Fe_2O_3 NPs, a Quantachrome NOVA 1200 was employed. The N_2 physisorption at 77 K (liquid nitrogen temperature) was carried out to obtain the N_2 adsorption results at different relative pressures (P/P_0) in the range of 0.05-0.35.

TGA analysis

A thermogravimetric measurement of the pre-calcined sample, of the synthesized Fe_2O_3 sample, and of the activated carbon samples was performed using a Mettler Toledo 850 instrument. The TGA curves were recorded at a temperature range of 25 - 900°C, and a heating rate of 15 °C/min. The TGA for the pre-calcined sample and the activated carbon sample were performed under an O_2 atmosphere with a flow rate of 15 ml/L, while the synthesized Fe_2O_3 samples were taken under an N_2 atmosphere with a flow rate of 15 ml/L.

UV-vis and FT-IR study

UV-Vis spectra of the synthesized Fe_2O_3 NPs sample were recorded at 500 – 700 nm using a UV/visible spectrophotometer, Varian Carry 1E. To prepare the UV-Vis analyzed solution, an amount of 0.5 mg dried powder Fe_2O_3 NPs sample was dissolved in pure ethanol using a sonicator. The FT-IR spectra of the synthesized samples were obtained using a Fourier Transform Infrared spectroscopy (FT-IR), Perkin Elmer system 2000. The dry powder was blended with KBr, grounded and pressed into a disk. The spectrum was recorded at 400-4000 cm^{-1}.

Result and Discussion

Size and morphology characteristics

The size and morphology of the synthesized Fe_2O_3 and GAC/Fe_2O_3 samples were investigated by using the BET and, recorded SEM/TEM images. Representative TEM images for the synthesized α-Fe_2O_3 nanoparticles were prepared in a different molar ratio of $FeCl_3$: NaOH as shown in Figure 1(a-b). The result shows that hematite nanoparticles were mainly obtained as granules with a quasi-spherical shape. With an increasing amount of NaOH precipitating agent (Fig. 1b), the particles changed to form an oval shape with apparent porosity.

For the GAC/Fe_2O_3 samples, the representative SEM image (Fig. 1d) shows that hematite nanoparticles were clearly deposited on the surface and in the voids. The deposited particles overlapped from one to another - similar to the flower-flake shape represented in Figure 1c.

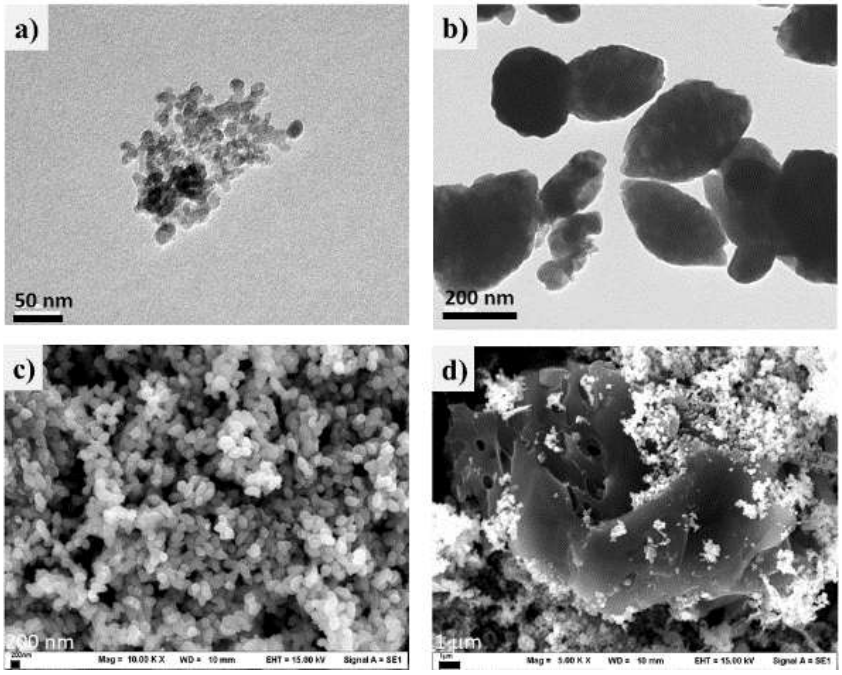

Figure 1.(a-b) TEM image of the synthesized Fe_2O_3 NPs a) S3 sample, b) S4 sample, and (c-d) SEM image of the synthesized iron oxide particles c) S4 sample, d) GAC/Fe2 sample

The specific surface area was calculated by the Brunauer–Emmet–Teller (BET) equation. Furthermore, the spherical particle size (d_{BET}) was estimated using Eq. (1) [32].

$$d_{BET} = \frac{6}{S_{BET} \times \rho_{th}} \qquad (1)$$

where ρ_{th} is the theoretical density of α-Fe_2O_3 (5.27 g/cm^3, [33]) and S_{BET} is the surface area reported by the BET measurement. The α-Fe_2O_3 particles were found in the range of 10 – 40 nm as shown in Table 2. The particle size was significantly varied due to the precipitating temperature and an amount of NaOH precipitating agent – a similar discussion has been observed in various other studies[25, 26, 28].

Table 2. **Result specific surface area, particle size, and production yield of α-Fe_2O_3 NPs**

Sample	Specific surface area (m^2/g)	Approximate particle size (nm)	Production Yield (%)
S1	32.91	34.78	79.59*
S2	108.32	10.57	43.55
S3	34.78	32.91	44.81
S4	114.24	10.02	58.96
S5	30.83	37.13	57.68
GAC/Fe1	3.78	-	75.67
GAC/Fe2	7.48	-	80.50
GAC/Fe3	3.07	-	79.60

***** the present amount may occur due to human error during the synthesis process.

TGA result

In order to find the optimum calcination temperature, thermogravimetric measurements for pre-calcined and GAC samples were performed under an O_2 atmosphere. The TGA curve results are shown in Figure 2a. For the pre-calcined sample, two steps of weight decomposition were revealed. Firstly, a temperature below 100°C due to the departure of water and solvent. Secondly, weight loss detected at 200-350°C can probably be assigned to the transformation of goethite (FeOOH) into hematite (α-Fe_2O_3). The transformation reaction can be written as illustrated in Eq. 2 [34]. In the case of the GAC sample, the TGA curve presents the onset temperature

of carbon degradation at ~350°C. Consequently, this observation allows us to specify the utmost calcination temperature at 350°C for both Fe_2O_3 NPs and GAC/Fe_2O_3 sample.

$2FeOOH\ (s) \rightarrow Fe_2O_3\ (s) + H_2O\ (g)$ (2)

The thermogravimetric measurements for the as-prepared α-Fe_2O_3 samples are illustrated in Figure 2b. The TGA curves for the synthesized α-Fe_2O_3 (black and red lines) present three distinct steps of mass loss. The first weight loss step was detected at less than 0.5 wt.% at 50 – 120°C. It could be contributed to the removal of water absorbed on the surface of the α-Fe_2O_3 particles. The second step revealed a minor weight loss (< 0.5 wt.%) occurring at the range of 450-550°C, which is in accordance with the transition phase of the synthesized compound [25, 26, 28]. The third weight loss was detected at a temperature above 700°C. Regarding Lassoued et. al. [25, 26, 28], the latter step was assigned to the high stability of the α-Fe_2O_3 nanoparticle. For the TGA curve of the activated carbon doped α-Fe_2O_3 nanoparticles (Fig. 2b, blue curve), two weight drops were presented. The first point at below 100°C was about 10 wt.% can be contributed to the absorbed water on the surface particle, especially the activated carbon. A further step was at 450-600°C, which was associated with the carbon decomposition. Accordingly, this allowed us to estimate the minimum amount of the doped α-Fe_2O_3 nanoparticle on activated carbon which is discussed in a further section.

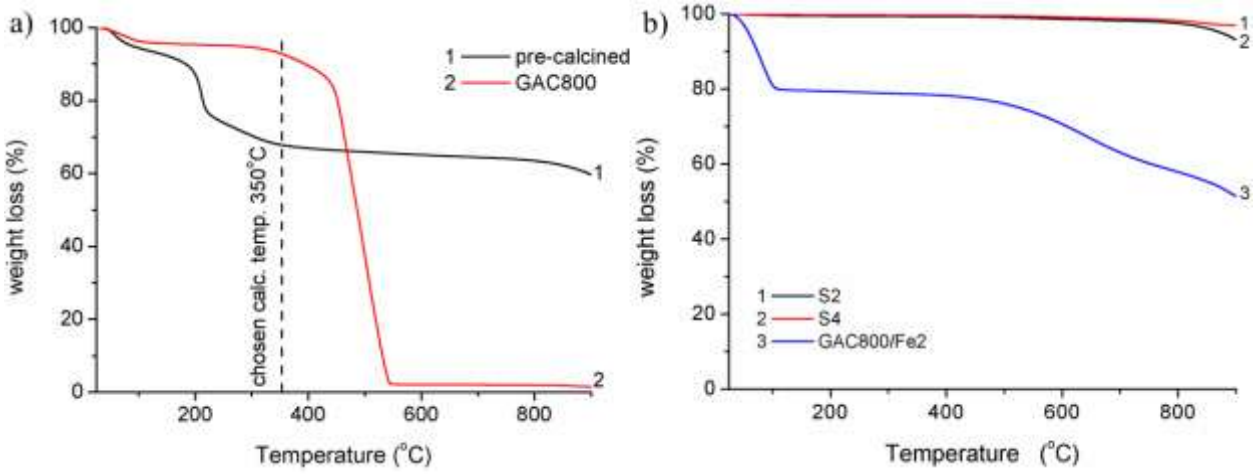

Figure 2.TGA curve of a) pre-calcined and GAC sample under O_2 atmosphere b) calcined Fe_2O_3 NPs (black and red curves) and GAC/Fe_2O_3 (blue curve) under an N_2 atmosphere

UV-vis and FT-IR spectroscopy result

Synthesized Fe_2O_3 nanoparticles which were prepared in different conditions were characterized by a UV-Vis spectrophotometer. The transmittance spectra were recorded in the range of 500-700 nm wavelength as shown in Figure 3a. This result coincided with the data from Lassoued et. al. [25]. The UV-vis transmittance spectra of the four different samples (Fig. 3a) was similar to those of the α-Fe_2O_3 phase overall. The spectra also had a noticeable red-shift with an increasing diameter of particles, likely contributed to the spatial confinement effect.

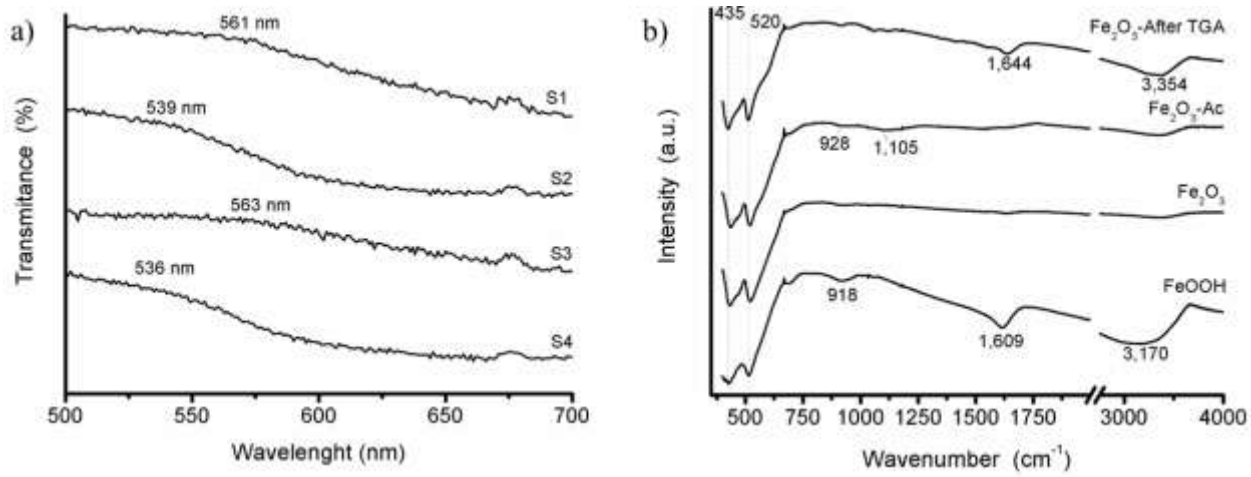

Figure 3.a) UV-visible spectra of iron oxide nanoparticles (Fe_2O_3 NPs) in distinct Fe: NaOH ratio and synthesized temperature b) FT-IR spectra of pre-calcined, synthesized Fe_2O_3, GAC/Fe_2O_3, and post-thermal treated Fe_2O_3 sample

Figure 3b illustrates the FT-IR spectra for pre-calcined, calcined, and GAC/F_2O_3 samples. For a pre-calcined sample, the spectrum could be well identified to the ferric oxyhydroxide compound which presented a very broad absorption band centred at 3,170 cm^{-1} and detected a peak at 1,609 cm^{-1}. These two bands could be assigned to the stretching and bending mode of the hydroxyl group and/or the water molecule [25, 35-37], respectively. In the case of the calcined samples, the strong absorption peaks at 435 and 520 cm^{-1} were observed due to the Fe-O bond vibrational mode [25, 26, 35, 36]. The spectrum confirmed a pure phase of α-Fe_2O_3 formation. In addition, it presented only a small amount of absorbed water on the powder's surface regarding the detected band at 3,245 cm^{-1}. In the case of the thermal treatment sample (after TGA at 900°C), intense absorption broad band centred at 3,354 cm^{-1} anda peak at 1,644 cm^{-1} were observed. It implies that the post-thermal treated hematite particles lead to a sorb facile moisture/water molecule.

Minimum Fe_2O_3 NPs doping and its production yield

The hematite product yield was calculated using Eq. 3 and is presented in Table 2. The result shows that the α-Fe_2O_3 production yielded about 40-60% in the case of the undoped GAC synthesis. The loss of fine particles mainly occurred in the separation and the purification process. In the case of the α-Fe_2O_3 doped on the granular activated carbon synthesis, the α-Fe_2O_3 product yield increased by about 1.5 times, 70-80%. It is probably because the fine particles were collected well and were deposited on the surface of the porous activated carbon.

$$Fe_2O_3 \text{ product yield (\%)} = \frac{\text{actual } Fe_2O_3 \text{ weight}}{\text{theoretical } Fe_2O_3 \text{ weight}} \times 100\% \quad (3)$$

According to the TGA results discussed in the previous section, the minimum α-Fe_2O_3 doping on granular activated carbon were only estimated. A plot between α-Fe_2O_3: the GAC weight ratio and the received α-Fe_2O_3 NPs weight percentage are shown in Figure 4. When the amount of the GAC sample was increased, the percentage of the deposited α-Fe_2O_3 weight decreased. However, the trade line of the amount of the α-Fe_2O_3 particles appeared to be in an equilibrium. It indicated that the minimum amount of α-Fe_2O_3 particles coated on the activated carbon was feasible at about 75 wt.%.

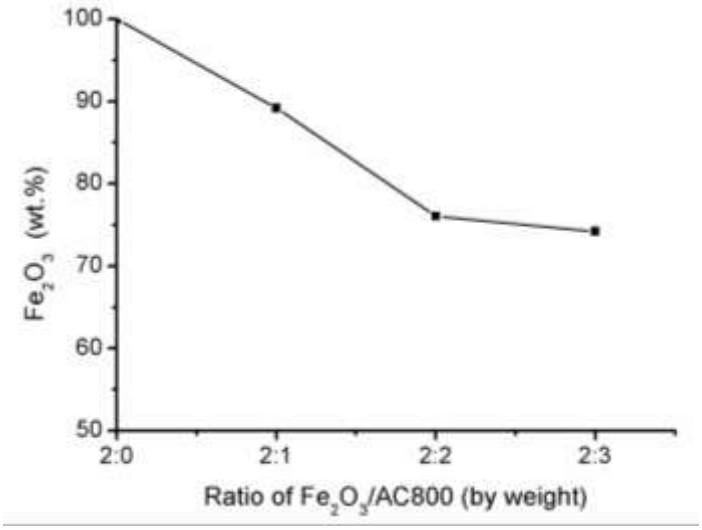

Figure 4.The weight percentage of Fe_2O_3 NPs coated on activated carbon

Conclusion

The α-Fe_2O_3 nanoparticles andthe α-Fe_2O_3 NPs coated on the granular activated carbon were well prepared by the facile chemical precipitation method. The suitable calcining temperature was revealed at 350°C. The particle size of the α-Fe_2O_3 NPs was approximately between 10 nm to 40 nm. The highest specific surface area of 115 m^2/g in ca. of the synthesis under 90°C with a 1:1.5 ratio of $FeCl_3$: NaOH. The particles mainly formed as granules with a quasi-sphere shape. However, the morphology characteristic changed to an oval shape when increasing the amount of the NaOH agent as well as the precipitating temperature. The α-Fe_2O_3 product yield in ca. when synthesized alone, produced α-Fe_2O_3 nanoparticles at about 40-70%. The yield increased to about 1.5 times when the granular activated carbon sample was added. The minimum weight percentage of the α-Fe_2O_3 NPs coated on the granular activated carbon was reported at about 75 wt.%.

Acknowledgements

The author would like to acknowledge Mrs. Naruporn Vasontarujiroj for helping in Laboratory. Moreover, the fiscal year's project for the undergraduate program in chemical engineering (Engineering faculty) is gratefully acknowledged for their financial support.

References

1. I. Enniya, L. Rghioui and A. Jourani, Sustainable Chemistry and Pharmacy, 7, 2018, 9-16.
2. M. Solgi, T. Najib, S. Ahmadnejad and B. Nasernejad, Resource-Efficient Technologies, 2017, 3, 236-248.
3. D. Huang, G. Wang, Z. Shi, Z. Li, F. Kang and F. Liu, Journal of Cleaner Production, 165, 2017, 667-676.
4. P. Luekittisup, V. Tanboonchauy, J. Chumee, S. Predapitakkun, R. W. Kiatkomol and N. Grisdanurak, Journal of Chemistry, 2015, 2015, 9 pages.
5. J. Lemus, M. Martin-Martinez, J. Palomar, L. Gomez-Sainero, M. A. Gilarranz and J. J. Rodriguez, Chemical Engineering Journal, 211-212, 2012, 246-254.
6. S. Cheng, L. Zhang, A. Ma, H. Xia, J. Peng, C. Li and J. Shu, Journal of Environmental Sciences, 65, 2018, 92-102.
7. P. Suresh Kumar, T. Prot, L. Korving, K. J. Keesman, I. Dugulan, M. C. M. van Loosdrecht and G.-J. Witkamp, Chemical Engineering Journal, 326, 2017, 231-239.
8. C. Chen, H. Chen, X. Guo, S. Guo and G. Yan, Journal of Industrial and Engineering Chemistry, 20, 2014, 2782-2791.
9. L. M. Kustov and A. L. Tarasov, Mendeleev Communications, 24, 2014, 349-350.

10. O. H. Ahmed, M. Altarawneh, Z. T. Jiang, M. Al-Harahsheh and B. Z. Dlugogorski, Chemical Engineering Journal, 323, 2017, 396-405.
11. M. A. Legodi and D. de Waal, Dyes and Pigments, 74, 2007, 161-168.
12. F. Froment, A. Tournie and P. Colomban, Journal Raman Spectroscopy, 39, 2008, 560-568.
13. D. Walter, Thermochimica Acta, 445, 2006, 195-199.
14. P. Pal, S. S. Syed and F. Banat, Bionanoscience, 7, 2017, 546-553.
15. S. H. Lee, H. Choi and K. W. Kim, Journal of Geochemical Exploration, 184, 2018, 247-254.
16. Z. M. Liu, J. T. Chen, Y. C. Wu, Y. R. Li, J. Y. Zhao and P. Na, Journal of Hazardous Materials, 343, 2018, 304-314.
17. G. Venkatesan and S. L. Narayanan, Chemical Engineering Communications, 205, 2018, 34-46.
18. T. Zhang, C. L. Zhu, Y. S. Shi, Y. Li, S. M. Zhu and D. Zhang, Materials Letters, 205, 2017, 10-14.
19. Q. Li, H. J. Wang, J. J. Ma, X. Yang, R. Yuan and Y. Q. Chai, Journal of Alloys and Compounds, 735, 2018, 840-846.
20. M. V. Reddy, C. Y. Quan and S. Adams, Materials Letters, 212, 2018, 186-192.
21. L. E. Mathevula, L. L. Noto, B. M. Mothudi, M. Chithambo and M. S. Dhlamini, Journal of Luminescence, 192, 2017, 879-887.
22. S. Boumaza, H. Kabir, I. Gharbi, A. Belhadi and M. Trari, International Journal of Hydrogen Energy, 2017.
23. M. Zhu, J. Kan, J. Pan, W. Tong, Q. Chen, J. Wang and S. Li, Journal of Energy Chemistry, 2017.
24. H. Katsuki, E.-K. Choi, W.-J. Lee, W.-S. Cho, K.-T. Hwang, W. Huang and S. Komarneni, Ceramics International, 43, 2017, 14050-14056.
25. A. Lassoued, B. Dkhil, A. Gadri and S. Ammar, Results in Physics, 7, 2017, 3007-3015.
26. A. Lassoued, M. S. Lassoued, B. Dkhil, A. Gadri and S. Ammar, Journal of Molecular Structure, 1148, 2017, 276-281.
27. A. Lassoued, M. S. Lassoued, B. Dkhil, A. Gadri and S. Ammar, Journal of Molecular Structure, 1141, 2017, 99-106.
28. A. Lassoued, M. S. Lassoued, B. Dkhil, S. Ammar and A. Gadri, Physica E: Low-dimensional Systems and Nanostructures, 97, 2018, 328-334.
29. L. L. Lin, S. A. Starostin, V. Hessel and Q. Wang, Chemical Engineering Science, 168, 2017, 360-371.
30. D. Lee, Y.-W. Choi, Y.-S. Na, S.-S. Choi, D.-W. Park and J. Choi, Materials Research Bulletin, 68, 2015, 221-226.
31. Q. Liu, C. Chen, G. Yuan, X. Huang, X. Lü, Y. Cao, Y. Li, A. Hu, X. Lu and P. Zhu, Journal of Alloys and Compounds, 715, 2017, 230-236.
32. R. F. K. Gunnewiek, C. F. Mendes and R. H. G. A. Kiminami, Advanced Powder Technology, 27, 2016, 1056-1061.
33. W. Zhu, J. Winterstein, I. Maimon, Q. Yin, L. Yuan, A. N. Kolmogorov, R. Sharma and G. Zhou, The journal of physical chemistry. C, Nanomaterials and interfaces, 120, 2016, 14854-14862.
34. H. B. Liu, T. H. Chen, X. H. Zou, C. S. Qing and R. L. Frost, Thermochimica Acta, 568, 2013, 115-121.
35. E. Darezereshki, Materials Letters, 65, 2011, 642-645.
36. X. R. Zhang, Y. G. Zhu, Y. Xie, Y. B. Shang and G. B. Zheng, Separation and Purification Technology, 186, 2017, 175-181.
37. D.-E. Zhang, X.-J. Zhang, X.-M. Ni and H.-G. Zheng, Materials Letters, 60, 2006, 1915-1917.

*****